Journal of Electron Spectroscopy and Related Phenomena 231 (2019) 127–139

Contents lists available at ScienceDirect

Journal of Electron Spectroscopy and Related Phenomena

journal homepage: www.elsevier.com/locate/elspec

Application of X-ray photoelectron spectroscopy to studies of electrodes in fuel cells and electrolyzers

K. Artyushkova[a,*], A. Serov[a,1], H. Doan[d], N. Danilovic[b,2], C.B. Capuano[b], T. Sakamoto[c], H. Kishi[c], S. Yamaguchi[c], S. Mukerjee[d], P. Atanassov[a]

[a] Department of Chemical & Biological Engineering, Center for Micro-Engineered Materials, University of New Mexico, Albuquerque, NM 87131, USA
[b] Proton on Site, Wallingford, CT 06492, USA
[c] R&D Division, Daihatsu Motor Co. Ltd., 3000 Yamanoue, Ryuo, Gamo, Shiga 520-2593, Japan
[d] Department of Chemistry and Chemical Technology, Northeastern University, Boston, MA 02115, USA

ARTICLE INFO

Article history:
Received 3 September 2017
Received in revised form 6 November 2017
Accepted 20 December 2017
Available online 21 December 2017

Keywords:
XPS
Fuel cells
Electrolyzers
Durability
Electrocatalysts
Catalyst layers

ABSTRACT

The activity and stability of catalysts used in anodes and cathodes in fuel cells and electrolyzers is a vital factor for practical industrial applications. To improve performance characteristics, it is essential to link the structure and composition of the catalyst on the electrodes to electrochemical performance and durability. The investigation of the durability of materials for application in fuel cells and electrolyzers is a particularly important task. Application of x-ray photoelectron spectroscopy (XPS) to probing the chemistry of catalyst layers and their degradation is becoming a central analytical approach due to quantitative chemical information it provides. Herein we present several cases of application of high-resolution XPS for analysis of the chemistry of electrodes and changes that are occurring during operation in several technological platforms, such as proton-exchange membrane fuel cells (PEMFCs), alkaline membrane fuel cells (AEMFC), direct methanol fuel cells (DMFC), direct hydrazine fuel cells (DHFC) and water electrolyzers (WE). Challenges of analyzing surface chemistry of electrodes and approaches to address them are discussed.

Contents

* Corresponding author.
E-mail address: kartyush@unm.edu (K. Artyushkova).
[1] Currently at Pajarito Powder, Albuquerque, NM 87102, USA.
[2] Currently at Energy Storage and Distributed Resources Division, Lawrence Berkeley National Laboratory, Berkeley, CA 94710, USA.

https://doi.org/10.1016/j.elspec.2017.12.006
0368-2048/

1. Introduction

Fuel cells are one of the fastest growing alternative energy sources as they are the most promising technologies for market penetration in automotive applications and different consumer areas [1]. In fuel cells, the chemical energy of the fuel, is being converted to electrical current. Fuel cells consist of an anode, a cathode, and an electrolyte that allows either positively charged hydrogen ions or negatively charged hydroxyls to move between the two sides of the fuel cell. There are many types of fuel cells, and they are mainly classified by the kind of electrolyte they employ and the type of fuel they use. Electrolyzers are a promising technology for hydrogen production by splitting the water into hydrogen and oxygen. Like fuel cells, electrolyzers consist of an anode and a cathode separated by an electrolyte. Electrolyzers function in different ways due to the different type of electrolyte material involved. This review presents several examples of the application of surface analysis to several types of low-temperature fuel cells including proton exchange and anion exchange membrane based cells, which utilize hydrogen, alcohol, and hydrazine as fuel, and electrolyzers.

In PEMFCs (Fig. 1a), hydrogen is being oxidized on the anode. Protons pass through a proton-conducting membrane made of perfluorosulphonic acid polymer to the cathode, at which protons, electrons, and oxygen are reacting to produce water.

In AEMFCs (Fig. 1b), KOH is used as a liquid electrolyte having very high conductivity. On the cathode, oxygen reacts with water to produce hydroxyl ions which move from cathode to anode through a hydroxyl-conducting membrane. Hydrogen is being oxidized on the anode to produce water and electrons.

Alcohols, such as ethanol and methanol, are energy-dense yet reasonably stable liquids at all environmental conditions, that are much easier to transport than hydrogen. Direct Alcohol Fuel Cells, such as direct methanol fuel cells (DMFCs) are types of the proton-exchange fuel cell (Fig. 1a) in which methanol is used as the fuel instead of hydrogen. DMFCs offer several advantages, such as low cost of fuel, ease of handling, transport, and storage.[2] In DMFCs, methanol is being oxidized on the anode producing protons, electrons, and CO_2. Protons move from anode to cathode through the same type of solid electrolyte as in hydrogen PEMFCs. Reduction of oxygen is occurring on the cathode side. Methanol crossover, in which methanol diffuses without reacting through a membrane and reaching cathode is a major factor in DMFC's inefficiency.

Another subtype of liquid fuel-based fuel cells is based on hydrazine as a fuel. Recently Daihatsu Motor has developed a method for safe storage of hydrazine in fuel tanks as a solid hydrazone form (> $CN–NH_2$) [2]. These fuel cells can operate both in alkaline and acid media. A breakthrough has been made with the utilization of anion exchange membranes in AFCs utilizing hydrazine as fuel. This approach is a modification of AEMFCs (Fig. 1b) in which the cathode catalyst reduces oxygen, producing hydroxyl ion which penetrates through the membrane to the anode. The anode catalyst oxidizes hydrazine in liquid KOH electrolyte producing water and nitrogen.

Another alternative energy market focused technology is hydrogen production from electrolysis of water [3,4]. The overall process is composed of hydrogen evolution reaction (HER) at the cathode and oxygen evolution reaction on the anode (OER) which can be implemented both in alkaline and proton-conducting modes (Fig. 1c and d) [5]. The primary constraint on the efficiency of electrolysis is the slow oxygen evolution reaction which is thermodynamically unfavorable. The enormous effort, therefore, is being devoted to developing more efficient OER catalysts as well as removal or decrease of precious metal content in the catalyst.

For testing the performance and stability of electrodes in the above discussed technological platforms, the membrane electrode assembly (MEA) is the key internal component. The MEA is composed of a membrane, anode and cathode catalyst layers (CL), and gas diffusion layers (GDL). The membrane can be hydroxyl-conducting (AEM) or proton-conducting (PEM) membrane depending if the chemistry of the technology is alkaline or acid, respectively. In one approach of making the electrodes, the catalyst layer is deposited on the gas diffusion layer, forming a gas diffusion electrode (GDE). The electrodes are then assembled with membrane into a 5-layer MEA. In another method, called a catalyst coated membrane (CCM), the catalyst layer is directly coated onto the membrane which is then assembled with GDLs on both sides of anode and cathode. The GDL usually has a carbon microporous layer (MPL) to minimize the contact resistance between GDL and catalyst layer.

The catalyst layer shown in Fig. 1e) consists of the catalyst material itself and ionomer which provides ionic conductivity. The chemistry of the catalyst layer has the most significant impact on overall fuel cell performance, and reactant and product balance. The stability of catalysts used in anodes and cathodes discussed in either fuel cells or electrolyzers is of vital importance for practical industrial applications [6]. In most cases, catalyst structure and composition change over time during reactions on electrodes. It is critical, therefore to relate the failure mechanism and losses in performance to changes in the structure or composition of the catalyst on the electrode.

The U.S. DOE has established durability-test protocols for FC's, which includes tests for electrocatalysts, electrocatalyst supports, chemical and mechanical tests of membranes [7]. Investigation of the durability of materials for application in FCs is a complex task [8]. Electrochemical testing is the primary way of studying the durability of electrodes during fuel cell testing. Electrochemical impedance spectroscopy (EIS) is well known to be a very useful tool towards assessing overall performance levels of an operating fuel cell and was adopted to investigate the degradation of the catalyst layer of an operating fuel cell [9]. Neutron imaging of water inside the fuel cell [10,11], in-situ tomography [12,13], and use of segmented cells [14,15] are among recently developed approaches [16]. The chemical composition of the catalyst layer and changes that occur during fuel cell operation are the subjects of study by spectroscopic analytical methods. The application of spectroscopy for these purposes is limited. Mass spectrometry has been used to monitor fuel cell exhaust [17]. Raman spectroscopy, including

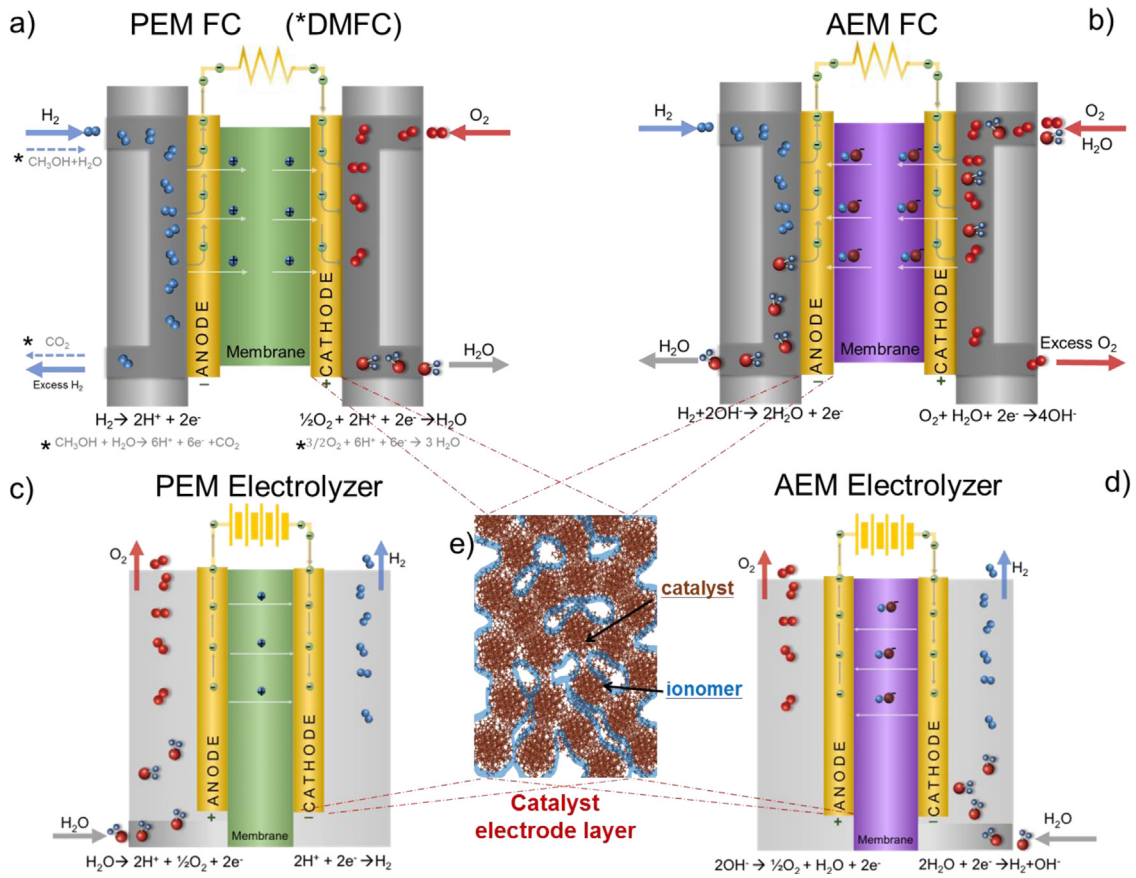

Fig. 1. Membrane electrode assembly for a) PEMFC, b) AEMFC, c) PEM electrolyzer, d) AEM electrolyzer. e) catalyst electrode layer, where the catalyst is mixed with an ionomer, is subject to surface analysis.

operando studies, was used to examine effects of degradation of fuel cell membranes [18,19]. Combination of XPS and synchrotron-based scanning transmission X-ray spectromicroscopy (STXM) was utilized to study cathode catalyst layers [20]. In situ/operando X-ray spectroscopic techniques such as ambient pressure X-ray photoelectron spectroscopy (APXPS) and X-ray adsorption spectroscopy (sXAS) are getting more and more attention [21].

Application of XPS to study catalyst layers and their degradation is becoming a routine analytical approach due to its chemical specificity, rich qualitative and quantitative information and accessibility [22–51]. In this review of recent work performed in our laboratory, we present application of high-resolution XPS for study of chemistry of electrodes and changes that are occurring during operation in several technological platforms, i.e. 1) anode for hydrogen oxidation reaction in AEM fuel cell, 2) cathode for oxygen reduction reaction in PEM fuel cell, 3) anode for methanol oxidation in direct alcohol fuel cell, 4) anode for hydrazine oxidation in direct hydrazine fuel cell and 5) anodes for oxygen evolution reaction in electrolyzer.

Current state-of-the-art fuel cells and electrolyzer systems rely on precious metal-based catalysts that make up a significant cost of the device. Replacing precious metals such as Pt and Ir by alternative platinum-group free (PGM-free) metals has been a worldwide initiative [52]. All materials used for cathodes and anode presented in this report are a part of our initiative in utilizing PGM-free materials.

2. Application example 1. Anode for hydrogen oxidation reaction in AEM fuel cell

Development of fuel cells based on using anion exchange membranes (AEMs) has drawn lots of interest in recent [28,36,39,40,49,53]. This technology allows a substantial decrease of the device cost by replacing expensive platinum catalysts on both cathode and anode by platinum group metal-free (PGM-free) catalysts. Over the last decade, several types of promising PGM-free catalysts have been developed for the AEMFC cathodes [36,38,40,41]. One of the systems that showed significant progress as an active material for hydrogen oxidation reaction (HOR) in alkaline media is Ni-based bimetallic systems with the second element being M = Mo, W, Cr, Cu, Zn, Sn, In or P and Se [54–56]. The role of metal on the electronic structure of the material, type of phases formed, shape and size of the particles all will affect the kinetics of hydrogen oxidation reaction.

We have recently reported the synthesis of NiMo catalysts supported on high surface area carbon as a highly active material for the HOR in alkaline media (anode catalyst in Fig. 1 b) [57]. The durability of the MEA fabricated with NiMo/KB anode catalyst was studied, and XPS was used to study changes in chemical composition of the electrodes after the test.

2.1. Experimental details

NiMo/KB catalyst was synthesized by thermal reduction of nickel and molybdenum precursors on the surface of Ketjen black (KB). The MEA cell was tested under the following conditions: H_2/O_2, T_{cell} = 70 °C, at a potential hold of 0.7 V to a maximum value of 55 mA/cm^2. Such an MEA activation procedure was performed for ~30 h. The cell was then held at constant voltage for 100 h. XPS was used to analyze the composition of a fresh MEA, and MEA after a test. XPS spectra were acquired on a Kratos Axis Ultra DLD X-ray photoelectron spectrometer using a monochromatic Al Kα source operating at 150 W. All powders and catalyst layers were conductive and mounted using conductive double-sided tape. No

use of charge neutralization was necessary, resulting in unambiguous peak positions of spectra for accurate peak identifications. Three areas for each sample were analyzed. High-resolution spectra were acquired at pass energies of 80 eV and 20 eV, respectively. Data analysis and quantification were performed using CasaXPS software. Sensitivity factors provided by the manufacturer were utilized. A 70% Gaussian/30% Lorentzian line shape was utilized in the curve-fit of spectra.

High-resolution Ni 2p, Mo 3d, O 1s and C 1s spectra were acquired. Ni 2p spectra were fitted using a combination of line shapes for Ni metal, NiO, $Ni(OH)_2$ developed by Biesinger et al [58]. and symmetrical peaks for mixed nickel molybdenum oxide at binding energy positions reported in the literature [59,60]. The microporous layer of GDL is a fluorinated carbon paper. After the test, a membrane with catalyst layer must be separated from the GDL to expose the electrode surface for analysis. A thin layer from the GDL can remain on the surface, contributing fluorine and carbon to the total signal detected by XPS. Fluorine Auger peaks contribute to the region of Ni 2p emission line. Mo 3d spectra were fit using reference positions for metallic Mo, various Mo oxides and mixed nickel molybdenum oxide NiMoOx as reported in the literature [58]. Higher oxidation state of the mixed oxide results in the contribution of the NiMoOx peak into higher binding energy value around 234 eV close to the Mo(VI) oxidation state of MoO_3.

2.2. Results

Fig. 2 shows high-resolution Ni 2p and Mo 3d spectra for the catalyst itself, fresh electrode and electrode after the test. The sampling depth of Mo 3d is 5 nm, while that of Ni 2p is 2.5 nm. XPS probes the very top surface of ~20 nm NiMo particles. Ni in the electrocatalyst has rich chemistry with some metallic component, oxidized form of Ni (NiO and $Ni(OH)_2$) and nickel-molybdenum oxide $NiMoO_x$. Molybdenum is present mainly as a mixed oxide with small amounts of Mo(IV), and Mo(V) detected. When electrocatalyst is incorporated into catalyst layer on the electrode by mixing it with anion-conducting ionomer and pressing into the assembly, some changes in chemistry are detected. The fresh electrode has 0.24 at% of Ni and 0.47 at% of Mo detected. Ni has a smaller amount of hydroxides with the more substantial relative amount of mixed nickel molybdenum oxides exposed to the surface, while Mo has only higher oxidation state with Mo(VI) and mixed nickel molybdenum oxides being major types of chemistries present. After the hold test, the atomic ratio of Ni/Mo increased dramatically from being 0.5 for the fresh electrode to 16. Segregation of Ni-rich phase to the top surface and loss of molybdenum (its concentration at the surface of the electrode after the hold test is 0.06%) can explain the increase of Ni at the surface to the surface.

In all MEAs, the catalyst layer is in contact with the gas diffusion layer (GDL The Ni 2p spectrum of the tested electrode in Fig. 2e) has broad features due to F Auger contribution. All of Ni oxide and hydroxide disappear during the hold test with mixed nickel molybdenum oxide being the primary type of Ni species preserved within the top 2.5 nm of the XPS sampling depth. The Mo that is left after the test is present in the mixed oxide state. The insignificant loss in activity observed during hold test shows that active $NiMoO_x$ phase is well preserved while inactive metal oxides are being removed during HOR.

3. Application example 2. cathode for oxygen reduction reaction in PEM fuel cell

Replacing platinum on the cathode for oxygen reduction reaction (ORR) the low-temperature proton exchange membrane (PEMFC) type of fuel cell by alternative materials is driven by the same considerations discussed above. Several classes of PGM-free catalysts exist. The most promising of these for the oxygen reduction reaction is based on metal-nitrogen-carbon (M-N-C, where M = Fe, Ni, Co, and Mn) composites. The durability data reported in the open literature reveals insufficient stability of this class of materials in real fuel cell tests. Recently, a catalyst with not only necessary activity for a commercially viable PGM-free ORR catalyst but also exhibiting high stability was reported [42]. In this example, we have used a catalyst synthesized from iron and nitrogen precursors as a cathode in PEMFC (Fig. 1a).

3.1. Experimental detail

The sacrificial support method (SSM) was used to synthesize this electrocatalyst from iron and nitrogen-carbon precursors. Synthesis and testing of electrodes for oxygen reduction reaction based on Fe-N-C catalyst materials were discussed in a recent report by Serov et al. [45]. The technology underlying the catalyst was invented by the University of New Mexico [42–44,61,62] and subsequently scaled-up and modified by Pajarito Powder, LLC. For the hold test, the load was applied potentiostatically to 0.65 V for 100 h at steady state. XPS analyzed fresh and tested electrodes. High-resolution N 1s, C 1s and O 1s spectra were acquired using the same experimental conditions as discussed in Section 1.

3.2. Results

Surface chemistry of MNC electrocatalysts for ORR and cathodes in PEMFC before and after fuel cell testing was analyzed (Fig. 3 a, c and e). Elements detected in catalyst itself are C, O, N, and Fe with 1.7 at% nitrogen and 0.6 at% iron.

Fig. 3a shows N 1s spectrum for the catalyst itself. A multitude of nitrogen types present has been discussed in the literature before [26,63]. Pyridinic N, N coordinated to Fe, hydrogenated N (such as pyrrolic or hydrogenated pyridine), graphitic N, cationic N^+ (quaternary and protonated nitrogen) and nitrous oxides are present in a catalyst with hydrogenated nitrogen being the most abundant type. When the catalyst is mixed with Nafion ionomer, a slight change in chemistry is evident (Fig. 3c) with a higher relative amount of higher binding energy peaks. The shift to the higher binding energy of the overall nitrogen photopeak is occurring due to the interaction of Nafion with catalyst and due to protonation of nitrogen moieties such as pyridinic nitrogen. After the hold test, the chemical composition of nitrogen changes very insignificantly (Fig. 3e). There is a slight decrease of total nitrogen detected at the surface of the tested electrode with a smaller amount of hydrogenated nitrogen detected. The unprecedented durability of these materials in ORR is directly related to the stable chemistry of the catalyst within the electrode.

4. Application example 3. Cathode for ORR and anode for methanol oxidation in direct alcohol fuel cell

The material from the same family of M-N-Cs has also been tested in a direct-alcohol fuel cell (DAFC). Highly active Fe-N-C catalyst derived from the pyrolysis of nicarbazin (a nitrogen charge transfer organic salt) and an iron precursor has been investigated. One of the biggest problems that engineers deal with in DAFCs is adsorption of alcohols, that can permeate through the membrane from anode to cathode, onto the active site of the conventionally used PGM-based catalyst. In this study, the Fe-N-C catalyst has demonstrated high tolerance towards both ethanol and methanol.

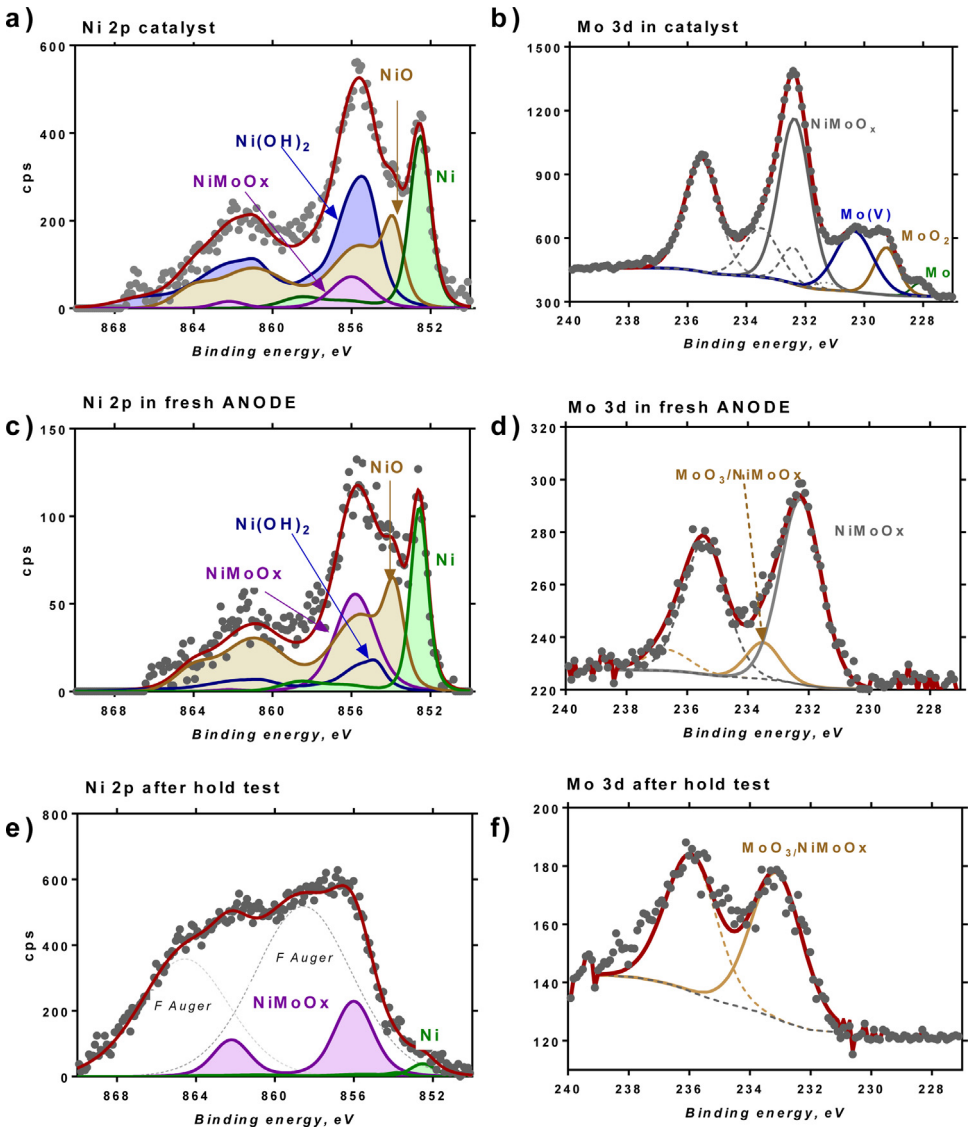

Fig. 2. High-resolution Ni 2p and Mo 3d spectra for NiMo HOR catalyst (a and b), fresh anode (c and d) and anode after hold test for 100 h (e and f).

4.1. Experimental details

Cathode electrodes were prepared using the PGM-free catalyst (Fe-NCB) as described previously [64,65]. Anode electrodes, based on PtRu black (Pt:Ru 1:1, Johnson Matthey), were prepared according to the procedure described in a previous report [13]. Durability tests were carried out in potentiostatic mode at 0.3 V and 90 °C, feeding 3 M methanol (DMFC) to the anode and fully humidified oxygen to the cathode under the same conditions of polarization experiments. XPS analyzed fresh and tested anodes and cathodes. High-resolution Pt 4 and Ru 3d spectra were fitted using Lorentzian asymmetric shape.

4.2. Results

The high-resolution N 1s spectra from the catalyst and fresh electrode are shown in Fig. 3 b) and d) are very similar to those from materials used in the ORR study discussed in example 2. After the test (Fig. 3 f), minimal changes are observed in the distribution of nitrogen species at the surface of the electrode. A slight decrease in the peak due to protonated nitrogen is accompanied by an increase in peaks due to species that serve as active sites for oxygen reduction – pyridinic nitrogen and nitrogen coordinated to the metal. Post-test analysis of anode side of the electrode assembly also revealed minimal changes in the chemistry of Pt and Ru with only slight reduction of Ru as shown in Fig. 4. Due to the contribution of carbon of GDL after separation of membrane assembly, there is an overall decrease in intensity of Pt and Ru in tested anodes, but the overall chemistry has not changed. In the fresh anode, mainly metallic Pt is present, and no changes in chemistry after the hold test are observed. Ru shows stability as preserved metallic Ru and RuO_2 phases in tested anodes.

5. Application example 4. Anode for hydrazine oxidation in direct hydrazine fuel cell

The final example of electrodes used in fuel cells shows post-test analysis of electrodes that were used in direct hydrazine hydrate fuel cells (DHFCs). DHFCs are one of the most promising candidates to enable complete PGM removal in anion exchange membrane (AEM) FCs by using non-platinum group metal (non-PGM) catalysts for both anode, and cathode [2,66].

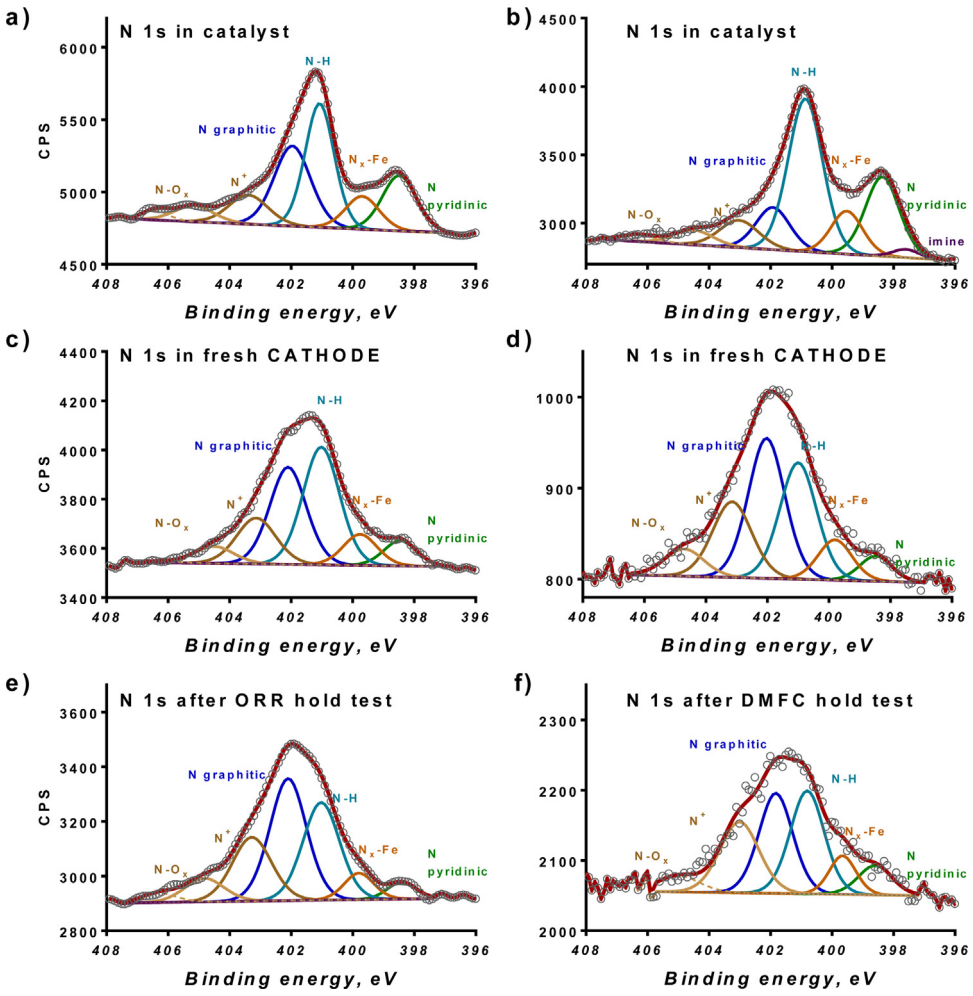

Fig. 3. High-resolution N 1s spectra for fresh M-N-C catalysts a) and b); fresh anodes c) and d); anodes after hold test e) and f) tested in ORR. PEMFC Application example 2 (a, c, e) and DMFC Application example 3 (b, d, f).

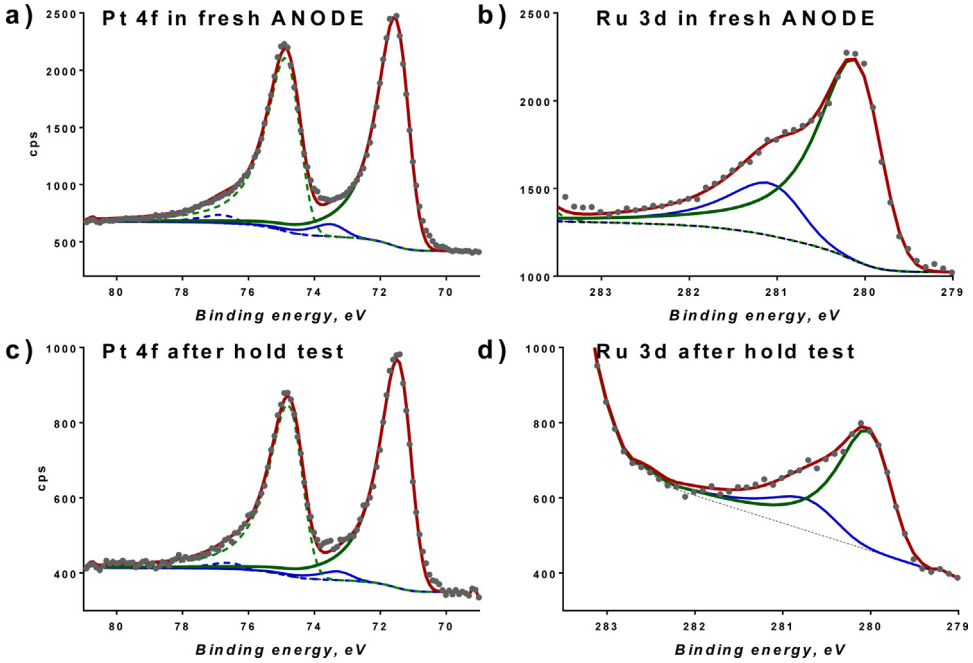

Fig. 4. High-resolution Pt 4f and Ru 3d (7/2 component) of the fresh PtRu anode (a and b) and anode after hold test (c and d) in DMFC Application example 3.

In this example, carbon supported Ni was used as an anode catalyst and Fe-AAPyr (AAPyr: aminoantipryne) was used as a cathode catalyst in AEMFC(configuration in Fig. 1b).

5.1. Experimental details

The preparation of anodic catalyst Ni/C was done by evaporation method as described in a previous report [66]. The same report describes the preparation of Fe-AAPyr cathode catalyst by SSM. The durability of DHFC was studied in the AEMFC configuration at 60 °C under original test protocol conditions developed by Daihatsu. The first test involved measuring the stability of AEM in 1% hydrazine hydrate for 350 h. The second test was a long-term test for 3500 h. XPS analyzed fresh and tested anodes and cathodes. High-resolution Ni 2p spectra were fitted based on the same lineshapes as discussed above.

5.2. Results

Table 1 shows changes in the elemental composition of cathode and anode and changes in chemical speciation of nitrogen and nickel after the short and long-term hold tests. Fig. 5 shows Ni 2p spectra for an anode and N 1s spectra for a cathode for fresh and two tested electrodes. Small amounts of F was detected at the surface of both fresh and tested anodes– less than 1% – resulting in single peak due to F Auger contributing into Ni 2p spectral region.

The increase in oxygen is a major change in elemental composition of both anode and cathode. Potassium was detected at the surface of both electrodes from the electrolyte. Cathode surface also showed a small presence of nickel due to migration from the anode. At the anode, reduction of nickel during the test was observed with a higher relative amount of metallic Ni detected at more extended hold times. In comparison with changes observed in the anode for hydrogen oxidation, the overall Ni chemistry is very well preserved. The stabilization of chemical changes during long-term operation as is evident from Fig. 6. The fresh cathode has a significant amount of cationic nitrogen N^+ such as protonated pyridine, protonated graphitic and quaternary nitrogen detected which are getting reduced during the first hour of the hold test and then the stable composition of the cathode is reached. The nitrogen chemistry of stabilized cathode is similar to the one seen above in the analysis of M-N-C materials for ORR and DMFC. Minor changes are observed in the chemistry of both electrodes demonstrating the high stability of these PGM-free materials in DHRC operation.

6. Application example 5. Anodes for oxygen evolution reaction in the electrolyzer

Oxygen evolution reaction (OER) electrocatalysis has received significant attention because of its prime role in water splitting. Traditionally, noble-metal-based materials have been utilized due to their stability at all pH values and high operating voltages. Iridium oxide (IrO_2) and ruthenium oxide (RuO_2) catalysts are considered the most active electrocatalysts for OER in PEM systems. The high cost and scarcity of these elements are major obstacles to widespread adoption in large-scale energy markets. Ni-based oxides have received significant attention for OER in AEM systems as the membranes and ionomers mature. Mixed metal oxides, with NiA_xO_y type of structure (A is metal) as discussed above for HOR, are being considered as important electrocatalysts for OER. The introduction of other metals such as Mo enhances the OER activity of NiO by improving the electric conductivity *via* modifying electronic structures. The stabilization of nickel during OER is another major challenge. Another group of the most promising and low-cost materials for electrolyzer technology is ternary metal oxides which possess multiple oxidation states that enable multiple redox reactions. Two ternary metal oxide systems have been tested in OER and surface chemistry of electrodes after the electrochemical test was analyzed by XPS.

6.1. Experimental details

Unsupported ternary Ni-Mo-Co catalysts were synthesized by the modified SSM adapted from the preparation of metal alloys [49,67,68]. The appropriate mixture of nickel and copper nitrates was dissolved in excess of water and added to the high surface area silica (Cab-O-Sil EH5, SA = 400m^2 g^{-1}). Ammonium molybdate was dissolved in water and solution was added drop-wise to a mixture of Ni, Co nitrates, and silica under vigorous mixing. The obtained colloidal dispersion of EH5 with precursors was dried in an oven at T = 85 °C for 8 h. The powder was ground with mortar and pestle and reduced in 7at% H_2, T = 550 °C, t = 1 h. Finally, silica was removed by dissolution in 7 M KOH for 8 h; the resulting unsupported catalyst material was washed with DI water until a neutral pH was obtained in the rinse water.

NiFeCo electrodes were synthesized by Northeastern University, also using the SSM method, by incorporating a strong reducing agent in the process [28]. The metal salts were calculated as followed: 2.39 g of $Ni(NO_3)_2{\cdot}6H_2O$, 412 mg of $Fe(NO_3)_3{\cdot}9H_2O$ and 300 mg of $Co(NO_3)_2{\cdot}6H_2O$ and dissolved with 20 mL of Mili Q water (18.2 MOhm) in 100 mL of silicon oxide (400 nm) dispersion solution. The silicon oxide dispersion solution was stored in a three-neck round bottom flask (RBF) and was sonicated overnight. The reduction step using $NaBH_4$ was performed by dissolving fresh $NaBH_4$ with 20 mL of Mili Q water and added dropwise to the silica/metal salts mixture. Nitrogen gas was bubbling through the reaction mixture as well during this process plus 30 min post-reduction. The solution was stirred overnight, and the process for the reduction step was repeated exactly as previously stated. After stirring overnight the second time, the solution was dried in vacuum oven at 80 °C for four days. The dried product was ball milled and heat treated in air for 3 h at 550 °C. The heat-treated product was etched with 7 M KOH for 48 h then washed with Mili Q water until the pH of the filter solution was neutralized to pH 7. Finally, the catalyst was dried at 80 °C in a vacuum oven overnight.

The catalyst powders were then used to manufacture gas diffusion electrodes (GDEs) for OER by Proton OnSite. The GDE's were prepared by mixing the catalyst powder into an ink containing solvents, ionomer (Tokuyama) or a non-functional binder (Nafion®). The stirred ink was sprayed using an airbrush onto a titanium porous transport layer (PTL) forming a GDE targeting a catalyst loading of 3 mg/cm^2. The cathodes used for membrane electrode assembly (MEA) testing under electrolysis conditions consisted of a Pt catalyst containing GDE manufactured under the same conditions as the anode GDE at a target loading of 3 mg/cm^2 onto carbon paper gas diffusion layer (GDL). Subsequently, an alkaline ionomer (Tokuyama) was airbrushed on top of the GDE. Electrolysis testing was performed using a modified 25 cm^2 Fuel Cell Technologies cell, where the graphite flow field on the OER side was replaced by a stainless steel parallel channel plate for stability at high potentials. The GDE's and membranes were exchanged in 0.5 M NaOH for one hour before testing. The cell was assembled by placing the appropriate GDEs on each side of an anion exchange membrane provided by Tokyama (A201). The MEAs were tested in electrolyzer conditions at T_{cell} = 50 °C with DI water feed containing 1 wt% of K_2CO_3, supplied on the anode side of the cell only. The cathode side was not pressurized, and no sweep gas was used; generated H_2 gas bubbled directly into a fume hood exhaust. In a typical test after the cell reached operating temperature, a polarization curve was carried out followed by a steady state test at 500 mA/cm^2 for 3 h to

Table 1
Elemental composition and relative composition of Ni for anode and N por cathode used in DHFC application example 4.

	C 1s%	O 1s%	Ni 2p%	F 1s%	K 2s%	Ni m%	NiO%	Ni(OH)2%
Anode fresh	87.5	10.1	2.3	0.2	0.0	1.7	55.9	42.4
Anode 350 h	83.5	11.2	2.6	0.7	2.0	4.9	49.6	45.5
Anode 3500 h	79.5	14.9	3.8	0.1	1.6	10.4	49.3	40.3

	C 1s%	O 1s%	N 1s%	F 1s%	K 2s%	Ni 2p%	N imine%	N pyrid%	N-Me%	N-H	Ngr	N^+	NO
Cathode fresh	95.6	3.6	0.9				2.6	12.9	16.5	25.1	5.9	34.1	3.0
Cathode 350 h	71.3	18.1	1.8	0.8	7.4	0.57	0.5	12.9	30.5	25.4	22.1	6.8	1.8
Cathode 3500 h	71.9	16.7	2.2	0.8	7.7	0.62	0.0	14.0	23.4	35.2	17.2	8.3	1.9

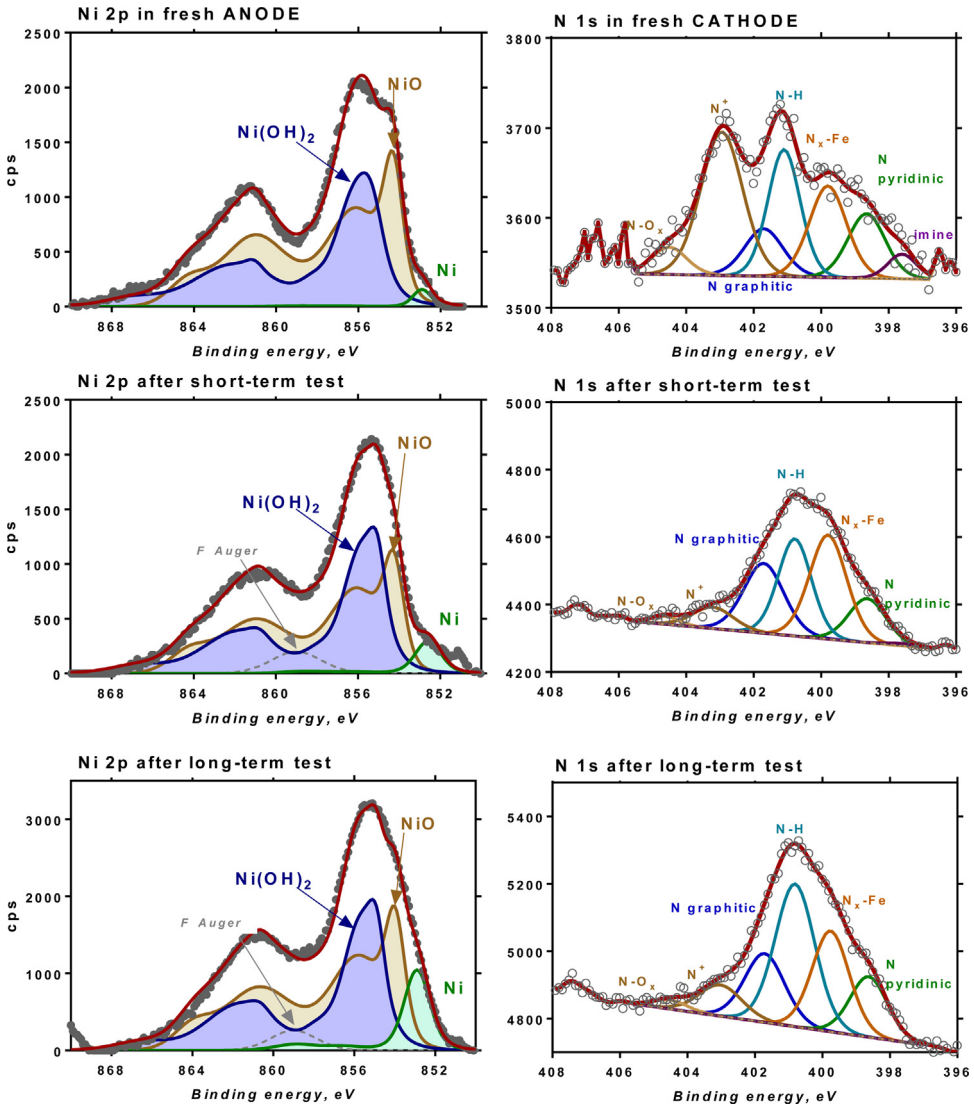

Fig. 5. High-resolution Ni 2p and N 1s spectra for fresh Ni/C anode a) and M-N-C cathode b); tested electrodes after short-term hold test – 350 h c) and d); and tested electrodes after long-term hold test 2–3500 h e) and f) discussed in Application example 4.

assess stability. The cell was then disassembled, and coupons were prepared for XPS analysis.

6.2. Results

Two alternative ternary oxides, NiMoCo and NiFeCo, have been tested in electrolysis mode in an MEA in comparison to reference platinum group metal-based electrodes (anode in Fig. 1d) as shown in Fig. 7. Two different ionomers were tested, one containing an alkaline ionomer from Tokuyama (baseline and NiMoCo), while NiFeCo was prepared with Nafion utilized as a binder. In comparison with Pt baseline, NiMoCo catalyst shows the same potential losses for all current densities. NiFeCo, which had Nafion as a binder, has very similar performance to baseline material at lower current densities but potential losses increase significantly as current density increases.

XPS evaluated the surface chemistry of the NiMoCo electrode containing electrocatalyst (Fig. 8 shows Ni 2p and Mo 3d spectra for fresh and tested anodes). The chemistry of NiMoCo catalyst layer in the fresh anode is very similar as in the HOR example discussed

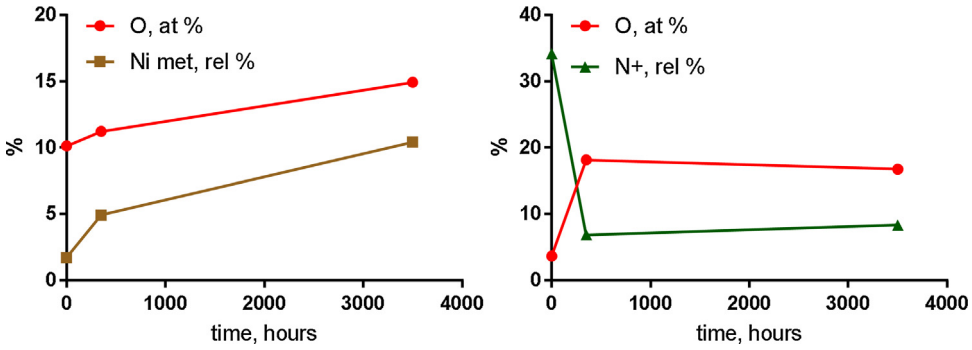

Fig. 6. Changes in the composition of anode – total oxygen and the relative amount of metallic Ni a) and for cathode – total oxygen and the relative amount of protonated nitrogen N^+ b) used in DHFC.

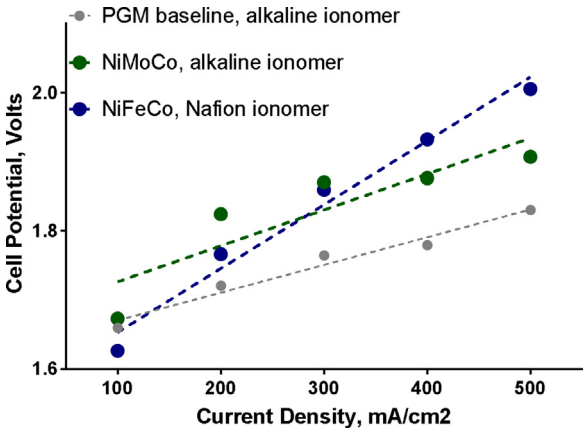

Fig. 7. Polarization curves are taken for MEAs containing specified anode/ionomer catalyst layers at 50 °C with a bicarbonate solution feed.

above in example 1. However, changes in the chemical composition of the electrode that are occurring during OER are different from the changes in HOR. During oxygen evolution reaction, Ni and Mo undergo severe oxidation, while Co was not detected. Half of the Mo is lost during the test, while nickel is preserved with significantly different chemistry.

A fresh NiMoCo electrode had 3at% of oxygen detected, while after electrolysis 33at% of oxygen is detected. Also, 1.3 at% of Ti and 6.8 at% of K was detected at the surface of the tested electrode. Ti comes from the porous transport layer, while K originates from the electrolyte. Nickel undergoes fundamental changes in chemical composition with most of metallic Ni being oxidized to hydroxide form. The peak due to mixed nickel molybdenum oxide is shifted to higher binding energy due to oxidation. This peak can also have a contribution from nickelate of contaminants such as potassium. The peak due to satellite has to be added in the Ni 2p spectrum due to higher contribution of Ni hydroxides into the total signal. Oxidation of mixed oxide phase is also evident from Mo 3d spectrum (Fig. 8d) which shows a significant decrease in intensity due to loss of Mo and shift to the higher binding energy of the molybdenum peak that is left due to oxidation.

Another ternary $NiFe_xCo_yO_z$ mixed catalyst was tested in the experiment for OER. Fig. 9 shows high-resolution Ni 2p spectra for electrocatalyst, fresh anode and tested anode while Table 2 shows elemental composition.

In fresh catalyst, Ni is a major element with Co and Fe present at 1:1 ratio on the order of 0.3–0.4 at%. The fresh electrode had F and S detected which are from the non-functional binder Nafion. A significant contribution of F Auger into Ni spectral region results in need of using two peaks. Upon mixing of the catalyst with the binder, the ratio of Co to Fe changes to Co being more dominant on the surface of the electrode than Fe. After the OER test, strong changes in composition are observed. Oxidation of the electrode is manifested by much higher oxygen detected. Ti from the porous transport layer and K from the electrolyte are detected in the tested electrode. Importantly, 0.4 at% of Pt was also detected due to cross-over of cathodic catalysts to the anode during operation. This is vital information that would not be available without surface analysis and which should not be ignored by the designers of electrolyzer systems.

In the tested electrodes, half the atomic% of Ni detected. The Fe is preserved while detection of Co is impossible due to overlap with Na 2s peak. The chemistry of nickel adds information on chemical changes that are occurring during OER. In the fresh electrode, the peak due to mixed alloy oxide is quite significant with Ni hydroxide being a second major phase present. After the test, more than third of hydroxide and oxide of Ni disappear with mixed alloy phase still being the most dominant. There is also a peak due to nickelate that is being formed. Oxidation of the electrode is not as severe for ternary $NiFe_xCo_yO_z$ oxide as for the binary NiMo material.

7. Discussion and perspective

The examples of applications of XPS to studies of the surface chemistry of PGM-free electrodes in fuel cells and electrolyzers show that XPS can provide an understanding of the surface chemistry in relation to performance at several levels:

7.1. The surface chemical composition of catalysts

The power of XPS is in its chemical sensitivity providing the quantitative chemical composition of synthesized materials. We have successfully derived speciation of Ni-based materials prepared for a variety of applications as supported single phase materials and as binary and ternary alloys with different metals. The role of alloying metal on the chemistry of catalysts was evaluated in relation to performance and stability in several technological applications. In comparison with single phase Ni-material (Fig. 5 a), the addition of Mo into the structure increased the amount of metallic Mo and decreased the amount of NiO significantly (Figs. 2a and 8a). Ternary NiFeCo alloy (Fig. 9), on the other hand, had a chemistry of nickel similar to the single-phase material. Importantly, the Ni-based material was active and stable as a catalyst for the anode in a hydrazine hydrate fuel cell, while similar in chemistry ternary NiFeCo material has demonstrated more significant performance losses in oxygen evolution reaction at higher current densities than NiMoCo-based systems.

XPS has been a critically important method of studying the chemistry of transition metal-nitrogen-carbon based composites for oxygen reduction. The progress made in interpretation of XPS N

Table 2
Elemental composition for $NiFe_xCo_yO_z$ catalyst, fresh and tested anode.

Sample	C 1s	O 1s	Ni 2p	Co 3p	Fe 3p	F 1s	K 2p	Pt 4f	S 2p	Si 2p	Ti 2p	*Co/Ni*	*Fe/Ni*	*Co/Fe*
FeCo cat	17.1	58.7	23.4	0.40	0.35							*0.017*	*0.015*	*1.157*
NiFeCo fresh Anode	28.4	17.9	7.5	0.29	0.08	45.2			0.62			*0.039*	*0.011*	*3.487*
NiFeCo anode after OER test	26.8	30.8	4.0	n/d	0.08	27.9	4.4	0.37	0.19	2.3	3.1			

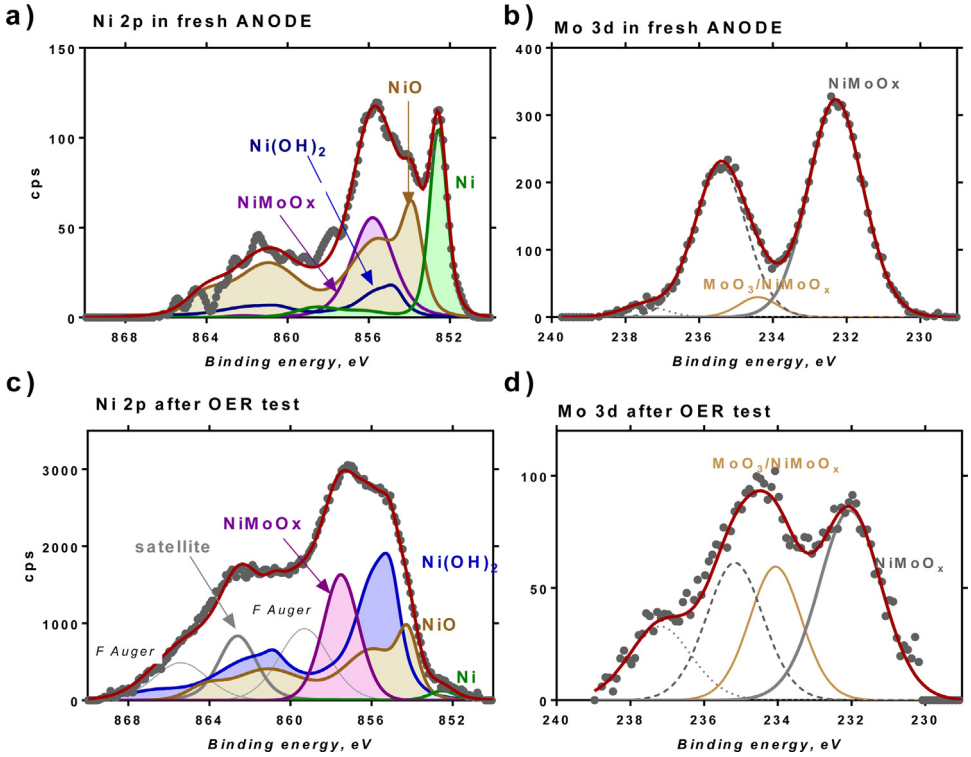

Fig. 8. High-resolution Ni 2p and Mo 3d spectra in fresh (a and b) and tested (c and d) NiMoCo anodes used in OER application example 5.

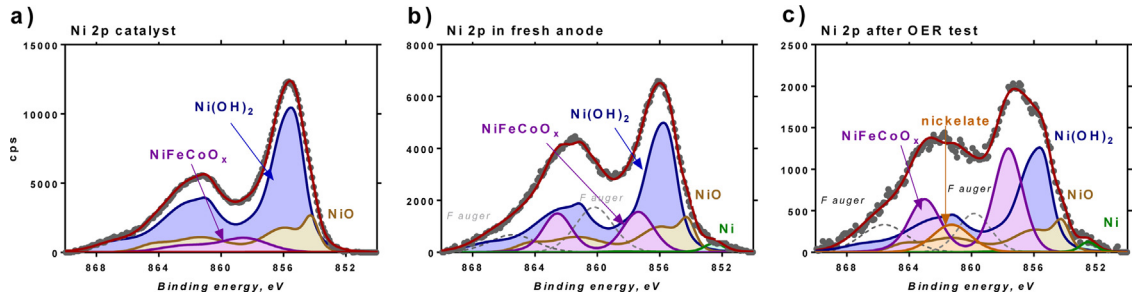

Fig. 9. High-resolution Ni 2p spectrum for $NiFe_xCo_yO_z$ catalyst (a), a fresh anode (b) and tested anode in OER (c) discussed in Application example 5.

1s spectra by using DFT calculations of core level shifts [63,69–71], detailed structure-to-property correlation of large family of M-N-C materials [26,72] and control over synthetic methodologies allowing synthesis of materials with different distribution of nitrogen species [42,73,74], allows building direct link between the chemistry of catalysts and activity of these complex heterogeneous multicomponent materials in oxygen reduction.

7.2. The link between the chemistry of catalyst and chemistry of electrodes

Next important step in building a direct link between structural properties of the catalyst and performance is understanding the transition of the chemistry of synthesized catalysts towards the chemistry of the anodes and cathodes upon introducing the ionomer and other constituents of electrodes and processing steps involved in the making of the electrode. Interaction of catalyst with ionomer contributes to the catalyst layer chemical composition, while processing steps such as hot pressing of the electrodes, deposition of top ionomer layers and other steps may change chemical structure and morphology of electrodes. This was demonstrated in all applications discussed in this report. When single-phase and mixed Ni-based systems are used to make electrodes with an alkaline ionomer, small differences are introduced into the chemistry of nickel at the surface of the electrode with a smaller amount of hydroxides and more considerable amount of mixed oxide detected (Figs. 2b and 5c). When Ni-based mixed alloys are prepared using Nafion ionomer, much larger changes are introduced (Fig. 9b) with the similarly suppressed contribution of hydroxide but enriched contribution of the mixed alloy into the overall chemistry of nickel.

The same is true for the chemistry of nitrogen in M-N-C ORR cathodes. Upon mixing of M-N-C catalyst with Nafion ionomer, significant changes in nitrogen chemistry as was observed (Figs. 3c and d, 5b) due to the interaction of Nafion with catalyst and protonation introduced. The interaction of M-N-C with ionomer depends on the chemistry of catalysts themselves, but it is the chemistry of the resulting catalyst layers in the cathode that should be evaluated in a relationship to the performance in the oxygen reduction.

7.3. Post-test analysis of electrodes

The changes in overall elemental composition and chemical speciation of the electrodes can be followed by analyzing the surface composition of electrodes after they have undergone tests in fuel-cell and electrolyzer conditions. The overall chemical composition can provide useful information on possible loss of material from the electrode due to chemical degradation, oxidation of electrode components, contamination by components of the device and possible crossover off elements from other electrodes. Chemical speciation provides useful information on phases that are least/most stable during electrochemical reactions on the surface of electrodes.

We have seen that in an alkaline fuel cell (Application example 1), most of the surface molybdenum is being lost and Ni oxides and hydroxides are the least stable types of Ni while mixed $NiMoO_x$ oxides are the most stable phase that supports activity during the long-term test. Similar behavior was observed when single-phase Ni system was used as the anode in DHFC in an alkaline electrolyte (Application example 4) with loss of Ni oxides and hydroxides observed at the early stage of the test. The oxidation and degradation of nickel anode were much smaller during the reaction of hydrazine oxidation than in hydrogen oxidation reaction.

The changes that were detected in Ni-based anodes during electrolysis are strikingly different (Application example 5). Severe anode oxidation occurred with most of the metallic Ni and mixed alloy phase decreasing and formation of the higher oxidation state of mixed oxide and nickelate of contaminants observed (Figs. 8 and 9).

Potassium from electrolyte was detected at the surface of anodes in both AEM DHFC test and OER test. Titanium from porous transport layer was another contaminant detected at the surface of anodes used in electrolyzer tests. Cross-over of elements from another electrode is critical degradation problem. XPS was sensitive to detect Ni migrated from anode side to the cathode side in the application of DHFC (Application example 4), while Pt was detected at the surface of OER anode due to detachment of Pt from the cathode side in electrolyzer (Application example 5).

Stability of chemistry cathodes for oxygen reduction reaction based on M-N-C materials was shown on several platforms – PEMFC (Application example 2), DMFC (Application example 3) and AEM DHFC (Application example 4). For example, XPS confirmed that methanol crossover which is a significant problem in the direct methanol fuel cell did not cause deterioration of M-N-C electrode. Very small changes in nitrogen chemistry were also observed in cathodes used in a hydrazine hydrate alkaline fuel cell.

Despite the power of surface and chemical sensitivity of XPS, there are some ***complications and challenges*** that we have to be aware in the analysis of electrodes for fuel cells and electrolyzer applications.

1. XPS sampling depth of different photoelectron lines with respect to the particle size should be taken into account when the atomic elemental composition is being interpreted. The use and interpretation of atomic ratios of elements should be done with great care as the ratio of elements obtained for core-shell type of particles which sizes are much larger than XPS probing depths may lead to erroneous conclusions of chemical surface enrichments and depletions.
2. When electrodes are being made from catalysts, the influence of processing steps may cause problems in assessing chemical composition of interest. Sometimes ionomers can be used as top layers masking the chemical composition of the electrode itself. Another consideration analysts have to take into account while interpreting XPS results obtained from electrode analysis, is the thickness of electrodes, which are usually 10–100 μm thick, much larger than XPS probing depth. Corroboration of the relationship between chemical composition and performance should be done along with the application of other spectroscopic and microscopic bulk analytical methods.
3. The other constituents, besides the catalyst, of the electrode, such as ionomer, may occupy up to 50% wt of the total electrode composition making detection within the electrode surface of dopants and alloying compounds at low concentrations difficult or impossible. After the test has been performed, the electrodes have to be separated from other components of MEA such as diffusion layers, membranes, etc. With XPS being extremely surface sensitive, the total probed signal will always have a contribution from the layers that were in contact with the surface of interest. As an example, we have discussed the contribution of fluorine into Ni 2p spectral line due to gas diffusion layer that was in contact with the electrode surface.

8. Conclusions

This review presents several examples of the application of XPS to understand the relationship between the chemistry of electrocatalysts, the chemical composition of electrodes and their durability in real fuel cell and electrolyzer tests. The power of XPS in providing readily quantifiable chemical information allows following the evolution of changes in the surface chemistry of the catalysts implemented within electrodes. XPS provides unique chemical quantitative information of chemistry of catalyst and electrodes that is invaluable for understanding the role of different types of chemical moieties in electrochemical reactions and degradation changes occurring. For a complete understanding of structural, morphological and chemical effects occurring at the electrodes during reactions at anodes and cathodes, combination of analytical techniques should be used, in which microscopic methods covering the range of physical scales – from nm to mm – and bulk spectroscopic and structural methods such as XAS, XRD and others should be utilized. This multi-technique analytical information which is complementary to the electrochemical testing is essential for designing more durable materials for energy-related applications.

Acknowledgements

Financial support of the DOE-EERE Hydrogen, Fuel Cells and Infrastructure Technologies Program is gratefully acknowledged. The projects reported are partially supported by DOE EERE program, Incubator Award DE-EE0006962", USA DoE DE-EE0000459 and NSF GRFP Grant No. 1418062. CNR-ITAE and Diahatsu collaborators

References

[1] DOE hydrogen and fuel cells annual merit review papers, Fuel Cells Bull. 2016 (2016) 11.
[2] K. Asazawa, et al., A platinum-free zero-carbon-emission easy fuelling direct hydrazine fuel cell for vehicles, Angew. Chem. Int. Ed. 46 (42) (2007) 8024–8027.
[3] M. Carmo, et al., A comprehensive review on PEM water electrolysis, Int. J. Hydrogen Energy 38 (12) (2013) 4901–4934.

[4] M. Wang, et al., The intensification technologies to water electrolysis for hydrogen production –A review, Renew. Sustain. Energy Rev. 29 (2014) 573–588.
[5] Y. Cheng, S.P. Jiang, Advances in electrocatalysts for oxygen evolution reaction of water electrolysis-from metal oxides to carbon nanotubes, Prog. Nat. Sci.: Mater. Int. 25 (6) (2015) 545–553.
[6] L. Dubau, et al., A review of PEM fuel cell durability: materials degradation, local heterogeneities of aging and possible mitigation strategies, Wiley Interdiscip. Rev.: Energy Environ. 3 (6) (2014) 540–560.
[7] USCAR FUEL CELL TECH TEAM CELL COMPONENT ACCELERATED STRESS TEST PROTOCOLS FOR PEM FUEL CELLS 2010, DOE EERE.
[8] J. Wu, et al., Diagnostic tools in PEM fuel cell research: part II, Int. J. Hydrogen Energy 33 (6) (2008) 1747–1757.
[9] M. Shaneeth, S. Basu, S. Aravamuthan, PEM fuel cell cathode catalyst layer durability: an electrochemical spectroscopic investigation, Chem. Eng. Sci. 154 (2016) 72–80.
[10] R. Mukundan, R.L. Borup, Visualising liquid water in PEM fuel cells using neutron imaging, Fuel Cells 9 (5) (2009) 499–505.
[11] Q. Meyer, et al., Effect of gas diffusion layer properties on water distribution across air-cooled, open-cathode polymer electrolyte fuel cells: a combined ex-situ X-ray tomography and in-operando neutron imaging study, Electrochim. Acta 211 (2016) 478–487.
[12] A. Pfrang, S. Didas, G. Tsotridis, X-ray computed tomography of gas diffusion layers of PEM fuel cells: segmentation of the microporous layer, J. Power Sources 235 (2013) 81–86.
[13] I.V. Zenyuk, et al., Investigating evaporation in gas diffusion layers for fuel cells with X-ray computed tomography, J. Phys. Chem. C 120 (50) (2016) 28701–28711.
[14] T.V. Reshetenko, J. St-Pierre, Study of acetylene poisoning of Pt cathode on proton exchange membrane fuel cell spatial performance using a segmented cell system, J. Power Sources 287 (2015) 401–415.
[15] D. Spernjak, et al., Characterization of carbon corrosion in a segmented PEM fuel cell, ECS Trans. 41 (1) (2011) 741–750.
[16] J. St-Pierre, et al., Modern fuel cell testing laboratory, in: C. Breitkopf, K. Swider-Lyons (Eds.), Springer Handbook of Electrochemical Energy, Springer Berlin Heidelberg, Berlin, Heidelberg, 2017, pp. 611–647.
[17] Joh, et al., Mass spectrometry of polymer electrolyte membrane fuel cells, J. Anal. Methods Chem. 2016 (2016) 9.
[18] M. Holber, P. Johansson, P. Jacobsson, Raman spectroscopy of an aged low temperature polymer electrolyte fuel cell membrane, Fuel Cells 11 (3) (2011) 459–464.
[19] I. Kendrick, et al., Operando raman micro-spectroscopy of polymer electrolyte fuel cells, J. Electrochem. Soc. 163 (4) (2016) H3152–H3159.
[20] V. Berejnov, et al., Probing platinum degradation in polymer electrolyte membrane fuel cells by synchrotron X-ray microscopy, Phys. Chem. Chem. Phys. 14 (14) (2012) 4835–4843.
[21] E.J. Crumlin, et al., X-ray spectroscopy of energy materials under in situ/operando conditions, J. Electron Spectrosc. Relat. Phenom. 200 (2015) 264–273.
[22] S.M. Andersen, R. Dhiman, E. Skou, X-ray photoelectron spectroscopy investigation on electrochemical degradation of proton exchange membrane fuel cell electrodes, J. Power Sources 282 (2015) 87–94.
[23] N. Andreu, et al., XPS investigation of surface reactivity of electrode materials: effect of the transition metal, ACS Appl. Mater. Interfaces 7 (12) (2015) 6629–6636.
[24] K. Artyushkova, et al., Structural correlations: design levers for performance and durability of catalyst layers, J. Power Sources 284 (2015) 631–641.
[25] K. Artyushkova, et al., Optimization of ink composition based on a non-platinum cathode for single membrane electrode assembly proton exchange membrane fuel cells, J. Power Sources 226 (Suppl. C) (2013) 112–121.
[26] K. Artyushkova, et al., Chemistry of multitudinous active sites for oxygen reduction reaction in transition metal?nitrogen?carbon electrocatalysts, J. Phys. Chem. C 119 (46) (2015) 25917–25928.
[27] V.B. Avakov, et al., Study of degradation of membrane-electrode assemblies of hydrogen-oxygen (air) fuel cell under the conditions of life tests and voltage cycling, Russ. J. Electrochem. 50 (8) (2014) 773–788.
[28] M.K. Bates, et al., Charge-Transfer effects in Ni–Fe and Ni–Fe–Co mixed-Metal oxides for the alkaline oxygen evolution reaction, ACS Catal. 6 (1) (2016) 155–161.
[29] M.R. Berber, et al., A highly durable fuel cell electrocatalyst based on double-polymer-coated carbon nanotubes, Sci. Rep. (2015) 16711.
[30] B. Bozzini, et al., Study of a proton exchange membrane fuel cells catalyst subjected to anodic operating conditions: by synchrotron-based scanning photoelectron microscopy (SPEM) and high lateral-resolution X-ray photoelectron spectroscopy, J. Power Sources 196 (5) (2011) 2513–2518.
[31] Y.-H. Cho, et al., Stability characteristics of Pt1Ni1/C as cathode catalysts in membrane electrode assembly of polymer electrolyte membrane fuel cell, Electrochim. Acta 59 (Suppl. C) (2012) 264–269.
[32] Y.-H. Cho, et al., The dependence of performance degradation of membrane electrode assembly on platinum loading in polymer electrolyte membrane fuel cell, Int. J. Hydrogen Energy 37 (3) (2012) 2490–2497.
[33] D. Dang, et al., In situ construction of Ir@Pt/C nanoparticles in the cathode layer of membrane electrode assemblies with ultra-low Pt loading and high Pt exposure, J. Power Sources 355 (2017) 83–89.
[34] J.K. Dombrovskis, A.E.C. Palmqvist, Recent progress in synthesis, characterization and evaluation of non-Precious metal catalysts for the oxygen reduction reaction, Fuel Cells 16 (1) (2016) 4–22.
[35] E. Guilminot, et al., Membrane and active layer degradation upon PEMFC steady-State operation: I: platinum dissolution and redistribution within the MEA, J. Electrochem. Soc. 154 (11) (2007) B1106–B1114.
[36] A. Ignaczak, et al., Oxygen reduction in alkaline media—a discussion, Electrocatalysis (2017) 1–11.
[37] Q. Jia, et al., Spectroscopic insights into the nature of active sites in iron–nitrogen–carbon electrocatalysts for oxygen reduction in acid, Nano Energy 29 (2016) 65–82.
[38] D. Malko, A. Kucernak, T. Lopes, Performance of Fe–N/C oxygen reduction electrocatalysts toward NO2–, NO, and NH2OH electroreduction: from fundamental insights into the active center to a new method for environmental nitrite destruction, J. Am. Chem. Soc. 138 (49) (2016) 16056–16068.
[39] Y. Meng, et al., Structure–Property relationship of bifunctional MnO2 nanostructures: highly efficient, ultra-Stable electrochemical water oxidation and oxygen reduction reaction catalysts identified in alkaline media, J. Am. Chem. Soc. 136 (32) (2014) 11452–11464.
[40] N. Ramaswamy, S. Mukerjee, Fundamental mechanistic understanding of electrocatalysis of oxygen reduction on pt and non-Pt surfaces: acid versus alkaline media, Adv. Phys. Chem. 2012 (2012) 17.
[41] A. Serov, et al., Original mechanochemical synthesis of non-Platinum group metals oxygen reduction reaction catalysts assisted by sacrificial support method, Electrochim. Acta 179 (2015) 154–160.
[42] A. Serov, et al., Nano-structured non-platinum catalysts for automotive fuel cell application, Nano Energy 16 (2015) 293–300.
[43] A. Serov, et al., Templated non-PGM cathode catalysts derived from iron and poly(ethyleneimine) precursors, Appl. Catal. B 127 (2012) 300–306.
[44] A. Serov, et al., Highly active and durable templated non-PGM cathode catalysts derived from iron and aminoantipyrine, Electrochem. Commun. 22 (2012) 53–56.
[45] A. Serov, et al., Highly stable precious metal-free cathode catalyst for fuel cell application, J. Power Sources 327 (2016) 557–564.
[46] S. Stariha, et al., Non-PGM membrane electrode assemblies: optimization for performance, Int. J. Hydrogen Energy 40 (42) (2015) 14676–14682.
[47] N. Tachibana, et al., XPS characterization for oxidation states of perovskite nanoparticles as oxygen reduction electrocatalysts, BUNSEKI KAGAKU 66 (1) (2017) 11–17.
[48] G. Wang, et al., X-ray photoelectron spectroscopy study of the degradation of Pt/ITO electrocatalyst in an operating polymer electrolyte fuel cell, Chem. Eng. Sci. 154 (2016) 81–89.
[49] A. Zalineeva, et al., Nano-structured Pd-Sn catalysts for alcohol electro-oxidation in alkaline medium, Electrochem. Commun. 57 (2015) 48–51.
[50] F.-Y. Zhang, et al., Quantitative characterization of catalyst layer degradation in PEM fuel cells by X-ray photoelectron spectroscopy, Electrochim. Acta 54 (16) (2009) 4025–4030.
[51] Y. Zhang, et al., Study of the degradation mechanisms of carbon-supported platinum fuel cells catalyst via different accelerated stress test, J. Power Sources 273 (Suppl. C) (2015) 62–69.
[52] Energy, D.o., *ElectroCat. DOE's Approach to PGM-Free Catalyst and Electrode R&D*. 2017: 21 st International Conference on Solid State Ionics.
[53] G. Merle, M. Wessling, K. Nijmeijer, Anion exchange membranes for alkaline fuel cells: a review, J. Membr. Sci. 377 (1) (2011) 1–35.
[54] S.T. Hunt, et al., Activating earth-abundant electrocatalysts for efficient, low-cost hydrogen evolution/oxidation: sub-monolayer platinum coatings on titanium tungsten carbide nanoparticles, Energy Environ. Sci. 9 (10) (2016) 3290–3301.
[55] S. Lu, Z. Zhuang, Electrocatalysts for hydrogen oxidation and evolution reactions, Sci. China Mater. 59 (3) (2016) 217–238.
[56] C.C.L. McCrory, et al., Benchmarking hydrogen evolving reaction and oxygen evolving reaction electrocatalysts for solar water splitting devices, J. Am. Chem. Soc. 137 (13) (2015) 4347–4357.
[57] S. Kabir, et al., Platinum group metal-free NiMo hydrogen oxidation catalysts: superior performance and durability in alkaline exchange membrane fuel cells, J. Mater. Chem. A 5 (46) (2017) 24433–24443.
[58] M.C. Biesinger, et al., X-ray photoelectron spectroscopic chemical state quantification of mixed nickel metal: oxide and hydroxide systems, Surf. Interface Anal. 41 (4) (2009) 324–332.
[59] J. Haetge, I. Djerdj, T. Brezesinski, Nanocrystalline NiMoO4 with an ordered mesoporous morphology as potential material for rechargeable thin film lithium batteries, Chem. Commun. 48 (53) (2012) 6726–6728.
[60] Z. Zhang, et al., Facile hydrothermal synthesis of NiMoO4@CoMoO4 hierarchical nanospheres for supercapacitor applications, Phys. Chem. Chem. Phys. 17 (32) (2015) 20795–20804.
[61] N.D. Leonard, et al., Modeling of low-Temperature fuel cell electrodes using non-Precious metal catalysts, J. Electrochem. Soc. 162 (10) (2015) F1253–F1261.
[62] B. Piela, et al., Highly methanol-tolerant non-precious metal cathode catalysts for direct methanol fuel cell, Electrochim. Acta 55 (26) (2010) 7615–7621.
[63] I. Matanovic, et al., Core level shifts of hydrogenated pyridinic and pyrrolic nitrogen in the nitrogen-containing graphene-based electrocatalysts: In-plane vs edge defects, J. Phys. Chem. C 120 (51) (2016) 29225–29232.
[64] D. Sebastián, et al., Nano Energy 34 (2017) 195–204.

[65] D. Sebastian, et al., Performance, methanol tolerance and stability of Fe-aminobenzimidazole derived catalyst for direct methanol fuel cells, J. Power Sources 319 (2016) 235–246.
[66] T. Sakamoto, et al., Highly durable direct hydrazine hydrate anion exchange membrane fuel cell, J. Power Sources 375 (2018) 291–299.
[67] A. Serov, et al., Highly-active Pd-Cu electrocatalysts for oxidation of ubiquitous oxygenated fuels, Appl. Catal. B-Environ. 191 (2016) 76–85.
[68] A. Serov, et al., Effect of precursor nature on the performance of palladium-cobalt electrocatalysts for direct methanol fuel cells, J. Power Sources 195 (1) (2010) 175–180.
[69] K. Artyushkova, et al., Oxygen binding to active sites of Fe-N-C ORR electrocatalysts observed by ambient-Pressure XPS, J. Phys. Chem. C 121 (5) (2017) 2836–2843.
[70] S. Kabir, et al., Binding energy shifts for nitrogen-containing graphene-based electrocatalysts –experiments and DFT calculations, Surf. Interface Anal. (2016) (p. n/a-n/a).
[71] S. Kabir, et al., Computational and experimental evidence for a new TM-N-3/C moiety family in non-PGM electrocatalysts, Phys. Chem. Chem. Phys. 17 (27) (2015) 17785–17789.
[72] K. Artyushkova, et al., Predictive modeling of electrocatalyst structure based on structure-to-property correlations of X-ray photoelectron spectroscopic and electrochemical measurements, Langmuir 24 (16) (2008) 9082–9088.
[73] M.J. Workman, et al., Platinum group metal-free electrocatalysts: effects of synthesis on structure and performance in proton-exchange membrane fuel cell cathodes, J. Power Sources 348 (2017) 30–39.
[74] M.J. Workman, et al., Fe-N-C catalyst graphitic layer structure and fuel cell performance, Acs Energy Lett. 2 (7) (2017) 1489–1493.